ROYAL SOCIETY
OF CHEMISTRY

PAPER

Check for updates

Computational and experimental search for potential polyanionic K-ion cathode materials†

Jingyang Wang, ‡[ab] Bin Ouyang, ‡[ab] Hyunchul Kim,[a] Yaosen Tian,[b] Gerbrand Ceder *[ab] and Haegyeom Kim *[a]

Discovering high-energy cathode materials is critical to construct K-ion batteries for practical applications. Owing to the great success of layered oxides in Li- and Na-ion systems, K layered cathodes have also been investigated in recent years. However, the much larger size of K^+ compared to Li or Na introduces strong K^+-K^+ interaction within the layer, which results in a sloped voltage profile thereby limiting the specific capacity and operating voltage. In contrast, polyanionic materials with a three-dimensional K^+ arrangement can effectively mitigate K^+-K^+ interaction. In this work, ten K polyanionic compounds with theoretical capacity >100 mA h g^{-1} are screened from the Inorganic Crystal Structure Database as potential cathode materials for K-ion batteries. Among the ten proposed compounds, $K_2MnP_2O_7$, $K_2Mn_2P_2O_7F_2$, $K_2Fe_2P_2O_7F_2$, and $K_6V_2(PO_4)_4$ with average voltage <4.5 V are synthesized and evaluated electrochemically. While the re-insertion of K into these compounds is not fully reversible, it may be related to the very high migration barrier that we compute for K ions. In addition, we show the successful synthesis of a series of $K_3V_{3-x}Cr_x(PO_4)_4$ ($x = 0, 1, 2, 3$) compounds. Among these, $K_3V_2Cr(PO_4)_4$ exhibits the largest reversible capacity, as revealed by the *in situ* investigation. Finally, we find that the redox couples in many of these compounds sit at remarkably high potential, even higher than in equivalent Li compounds, which brings both opportunities and challenges in the future research of K polyanion cathodes.

Introduction

Since the first commercialization of lithium-ion batteries (LIBs) by Sony in the early 1990s, LIBs have been the primary technology to provide energy storage in portable electronic devices and electric vehicles (EVs). However, the skyrocketing demand for energy storage, especially in the emerging EV market, raises concern about the availability and cost of lithium and other metals used in Li-ion cathodes.[1–3] Na-ion batteries (NIBs) and K-ion batteries (KIBs) have been identified as potential low-cost alternatives to LIBs because of the natural abundance and wide distribution of Na and K resources. Compared to NIBs, KIBs are particularly attractive because (1) the standard redox potential of K/K$^+$ (−2.93 V *vs.* standard hydrogen electrode (SHE)) is lower than that of Na/Na$^+$ (−2.71 V *vs.* SHE), translating into a higher operating voltage in an electrochemical cell;[4] (2) the availability of stable K–graphite compounds enables the use of the well-developed graphite anode, while Na cannot

intercalate into graphite;[5,6] and (3) K$^+$ has higher mobility than Li$^+$ and Na$^+$ in organic liquid electrolytes.[7,8]

In the early stage of K-ion cathode development, layered oxide compounds attracted significant attention given their success in LIBs and NIBs. Many K-containing layered oxides have shown reversible electrochemical (de)intercalation of K ions, including K-deficient K_xMnO_2, K_xCoO_2, $K_xFe_{0.5}Mn_{0.5}O_2$, and $K_{2/3}Ni_{2/3}Te_{1/3}O_2$ ($x < 1$) and stoichiometric $KCrO_2$.[9–16] However, the average operating voltage is only in the range of 2.5 V *vs.* K/K$^+$ in most K layered oxides; the exception is $K_{2/3}Ni_{2/3}Te_{1/3}O_2$ in which electronegative TeO_6^{6-} moieties increase the working voltage to ∼3.3 V, but degrade the specific capacity.[17] In recent work, we furthermore concluded that layered K-oxide compounds intrinsically have sloped voltage profiles regardless of the transition metal chemistry.[8,18] In a layered structure, the large ionic radius of the K ion expands the alkali-ion layer and increases the interlayer distance, thereby making the screening from the adjacent oxygen layers less effective. The strong resulting K$^+$–K$^+$ interaction increases the steepness of the voltage profiles in the sense that the (de)intercalation occurs over a much wider voltage range, which often exceeds the electrolyte stability window, therefore limiting the achievable capacity and lowering the average voltage.[4,8,18–21]

Because of these issues with layered oxide compounds, polyanionic compounds are of more interest for K cathodes.[20,22–34]

[a]Materials Sciences Division, Lawrence Berkeley National Laboratory, Berkeley, CA 94720, USA. E-mail: haegyumkim@lbl.gov; gceder@berkeley.edu

[b]Department of Materials Science and Engineering, University of California, Berkeley, CA 94720, USA

‡ Equal contribution.

The larger K^+–K^+ distance in polyanionic compounds considerably reduces the effective K^+–K^+ interaction, generating a less sloped voltage profile and a generally higher operating voltage.[8,19,20] In addition, polyanion groups further increase the voltage *via* the inductive effect.[35] Indeed, several K polyanion compounds have recently been investigated as high-voltage cathodes. For instance, the $FeSO_4F$ framework can intercalate K^+ ions in a K half-cell at an average voltage of 3.6 V.[32] Park *et al.* performed an extensive screening of K polyanion cathodes in the K–M–O and K–M–P–O spaces, and identified KVP_2O_7 as a candidate with reasonable electrochemical performance (55 mA h g^{-1} at ~4.2 V).[26] In addition, the $KVPO_{4+x}F_{1-x}$ solid solution was investigated by Chihara *et al.*; this cathode material was shown to deliver a discharge capacity of 92 mA h g^{-1} at an average voltage of 4.13 V.[27] Kim *et al.* later demonstrated that the operating voltage and specific capacity of the $KVPO_{4+x}F_{1-x}$ system could be further improved to 4.33 V and 105 mA h g^{-1} by optimizing the synthesis route to obtain the end member $KVPO_4F$ in which two oxygens in the VO_6 octahedra are fully substituted by fluorine.[20] Recently, $KTiPO_4F$ was reported to have an average voltage of 3.6 V, which is extraordinarily high for $Ti^{3+/4+}$ redox,[34] further demonstrating that K-containing polyanions have the potential to provide high energy density by upshifting the working voltage. In addition to compounds made by conventional solid-state or sol–gel synthesis, meta-stable polyanion compounds such as $K_3V_2(PO_4)_2F_3$ can be obtained from their Na counterparts by electrochemical ion exchange.[25]

As part of a continuous effort to develop high energy K-ion cathode materials, we conduct in the current study a computational materials screening through the Inorganic Crystal Structure Database (ICSD) and identify 10 potential polyanionic K-ion cathode materials with theoretical capacity >100 mA h g^{-1}. Among the 10 candidates, 4 compounds (**$K_2MnP_2O_7$, $K_2Mn_2P_2O_7F_2$, $K_2Fe_2P_2O_7F_2$,** and **$K_6V_2(PO_4)_4$**), for which the theoretical average voltage is within a stable voltage window of the typical K-electrolytes (3.0–4.5 V), were synthesized and evaluated electrochemically. **$K_3Cr_3(PO_4)_4$** also appeared in the screening as a K-ion cathode material; however, its predicted average voltage was too high (>4.5 V). To lower the operating voltage to a practical electrochemical window, we successfully substituted Cr with V and investigated the K-ion storage properties in the $K_3V_{3-x}Cr_x(PO_4)_4$ ($x = 0, 1, 2, 3$) system. Among the $K_3V_{3-x}Cr_x(PO_4)_4$ compounds, $K_3V_2Cr(PO_4)_4$ exhibits the highest reversible discharge capacity of ~42 mA h g^{-1} with an average voltage of ~3.95 V and could maintain ~90% of the initial capacity after 50 cycles. The reversible structural evolution and $V^{3+/4+}$ redox reaction in this compound family was investigated using *in situ* X-ray diffraction (XRD) and X-ray absorption spectroscopy (XAS).

We find that redox potentials in many K-polyanion compounds sit on average at even higher voltage than in similar Li compounds. While this would benefit the specific energy of these cathode materials, combined with the poor K-ion mobility that we find, it will challenge the anodic limit of current K-ion electrolytes.

Experimental

Solid-state synthesis

$K_2Fe_2P_2O_7F_2$ was prepared by the solid-state reaction from a stoichiometric mixture of KF (>99%, Sigma-Aldrich) and $Fe_2P_2O_7$ in a sealed stainless steel tube at 600 °C for 16 h. To synthesize $Fe_2P_2O_7$, stoichiometric amounts of Fe_2O_3 (>96%, Sigma-Aldrich) and $NH_4H_2PO_4$ (98%, Alfa Aesar) were mixed and pre-heated at 350 °C before annealing at 900 °C under a continuous flow of H_2(2%)/Ar(98%) mixed gas for 12 h.

$K_2Mn_2P_2O_7F_2$ was prepared by a solid-state reaction from a stoichiometric mixture of KF (>99%, Sigma-Aldrich) and $Mn_2P_2O_7$ in a sealed stainless steel tube at 650 °C for 12 h. $Mn_2P_2O_7$ was prepared by decomposition of $MnPO_4$–H_2O (99%, Alfa Aesar) at 600 °C under continuous Ar flow for 3 h.

$K_2MnP_2O_7$ was synthesized by a solid-state reaction from a stoichiometric mixture of K_2CO_3 (anhydrous, VWR), MnO (99%, Alfa Aesar), $NH_4H_2PO_4$ (98%, Alfa Aesar), and 5 wt% carbon black (Super P, Timcal). The precursors were homogeneously mixed by wet ball-milling using acetone as a solvent and then dried at 90 °C on a hot plate. The mixture was pre-heated at 350 °C before annealing at 600 °C under continuous flow of Ar for 12 h.

$K_6V_2(PO_4)_4$ was prepared by a solid-state reaction from a homogeneous mixture of K_3PO_4 (98%, Sigma-Aldrich) and VPO_4 at 800 °C under continuous Ar flow for 8 h. VPO_4 was synthesized by reacting $NH_4H_2PO_4$ (98%, Alfa Aesar), V_2O_5 (>99.6%, Sigma-Aldrich), and 5 wt% carbon black (Super P, Timcal). The precursors were mixed using wet ball-milling in acetone for 12 h and dried overnight at 100 °C. The mixture was pelletized and then sintered at 750 °C for 4 h under continuous Ar flow.

To prepare $K_3V_{3-x}Cr_x(PO_4)_4$ ($x = 0, 1, 2, 3$) compounds, VPO_4 and $CrPO_4$ were synthesized to be used as precursors. Stoichiometric amounts of V_2O_5 (98%, Sigma-Aldrich) and $HN_4H_2PO_4$ (98%, Alfa Aesar) were homogeneously mixed with 5 wt% carbon, and the mixture was pelletized and sintered at 750 °C under Ar flow for 4 h to produce VPO_4. For the synthesis of $CrPO_4$, $Cr(NO_3)_3$–$9H_2O$ (99%, Sigma Aldrich) was dissolved in 60 mL of deionized water and $NH_4H_2PO_4$ (98%, Alfa Aesar) was dissolved in 10 mL of deionized water. The two solutions were mixed and dried. Then, the dried powder was pelletized and sintered at 1000 °C for 4 h in air. To synthesize $K_3V_{3-x}Cr_x(PO_4)_4$ ($x = 0, 1, 2, 3$) compounds, a stoichiometric amount of K_3PO_4 (anhydrous, >98%, Sigma-Aldrich) was homogeneously mixed with VPO_4 and $CrPO_4$. The mixture powder was pelletized and then sintered at 900 °C for 4 h under a continuous flow of H_2(2%)/Ar(98%) mixed gas. After natural cooling to 300 °C, the samples were kept at this temperature and then transferred to an Ar-filled glovebox to prevent contamination from moisture.

Characterization

The crystal structures of the obtained materials were analyzed using XRD (Rigaku Miniflex 600) with Cu Kα radiation. *In situ* XRD was performed on a Bruker D8 Advance X-ray diffractometer using Mo Kα radiation. A homemade *in situ* cell with a Be

This journal is © The Royal Society of Chemistry 2021

J. Mater. Chem. A, 2021, **9**, 18564–18575 | **18565**

window was galvanostatically cycled at 3 mA g^{-1} between 2.5 and 5.0 V using a Maccor potentiostat, and XRD patterns were collected from 13° to 22° 2θ every 30 min at room temperature. The particle morphology was verified using field-emission scanning electron microscopy (FE-SEM; Zeiss Gemini Ultra-55).

X-ray absorption spectroscopy (XAS) measurements were performed in transmission mode at room temperature at beamline 20-BM at the Advanced Photon Source, Argonne National Laboratory. The prepared XAS samples were sealed with polyimide tape (Kapton, DUPONT) to prevent contamination from air exposure. The incident energy was selected using a Si(111) monochromator, and the beam intensity was reduced by 15% using a Rh-coated mirror to minimize high-order harmonics. Reference spectra of V and Cr were collected using pure V and Cr metal foils. The XAS data were analyzed using Athena software, and the spectral energies were calibrated by referencing the first inflection points in the spectra of V and Cr metal foils.

Electrochemical tests

Cathodes were prepared by mixing $K_3V_{3-x}Cr_x(PO_4)_4$ (70 wt%), Super P carbon (Timcal, 20 wt%), and polytetrafluoroethylene binder (DUPONT, 10 wt%) in an Ar-filled glovebox. Cathodes with a loading density of ~3.7 mg cm^{-2} were assembled in a two-electrode configuration using a K-metal anode and glass fiber separator (Whatman, GF/F) in a 2032 coin cell. The electrolyte was custom-made using 0.7 M KPF$_6$ (Sigma-Aldrich) in anhydrous ethylene carbonate/propylene carbonate (EC/PC) (1 : 1 by volume, Sigma-Aldrich). Electrochemical tests were performed on a battery testing station (Arbin Instruments) at room temperature in galvanostatic mode. All the other electrodes were also tested under the same conditions.

Computational details

The DFT calculations were performed using the Vienna *ab initio* simulation package (VASP)[36] and projector-augmented wave (PAW) method.[37] For each of the structural optimization calculations, a reciprocal space discretization of 25 Å^{-1} was applied, and the convergence criteria were set to 10^{-6} eV for electronic loops and 0.02 eV Å^{-1} for ionic loops. The Perdew–Burke–Ernzerhof (PBE) exchange–correlation functional with the rotationally averaged Hubbard U correction[38] was applied to obtain more accurate DFT energetics; the U parameters were taken from a previously reported calibration to oxide formation energies.[39] For each of the compounds, multiple K-vacancy orderings were enumerated at different K concentrations, with the 20 configurations with the lowest electrostatic energy selected for DFT calculations. For compounds with mixing of cation or anion sites, the lowest energy cation/anion ordering in the pristine state was first determined. For other K contents, the enumeration was only performed on K/Vac sites with the cation/anion ordering fixed. The voltage profile was calculated from the DFT energies of materials on the pseudo-binary convex hull with the pristine compound and full depotassiated compound as the end compounds. The average between two K compositions x_1 and x_2 was determined as specified by Aydinol *et al.*:[40]

$$V = -\frac{E(K_{x_2}X) - E(K_{x_1}X) - (x_2 - x_1)E(K)}{(x_2 - x_1)F}, \qquad (1)$$

where $E(K_xX)$ and $E(K)$ are the DFT energies of the most stable $E(K_xX)$ and bcc K metal (space group: $Im\bar{3}m$), respectively, and F is the Faraday constant. Climbing image nudged elastic band (ci-NEB) calculations are performed to evaluate the K diffusion barrier for selected compounds.[41] For all calculations, the force convergence criterion is set to 0.05 eV Å^{-1}.

Results

Computational materials screening of ICSD for potential polyanionic K-ion cathodes

The computational materials search followed the criteria summarized in Fig. 1. K-containing polyanionic materials with composition A–TM–XO–C, where A represents K, TM represents one or more transition metals with multi-electron redox capability (from the group of V, Cr, Mn, Fe and Ni), XO represents a polyanion group (including PO_4^{3-}, SO_4^{2-}, SiO_4^{4-}, and BO_4^{5-}), and C represents the counter anion F$^-$ or O^{2-} (the presence of a counter anion was not required), were first identified in the ICSD,[42] resulting in a total of 74 K-containing polyanion compounds. Of these compounds, 20 compounds having a K/TM ratio <1 were excluded as they were unlikely to deliver high capacity. To ensure active redox centers, the remaining 54 candidates were reduced to 21 compounds by requiring that the transition metal is in octahedral coordination and has an appropriate valence state (*i.e.*, V^{3+}, Cr$^{2+/3+}$, Mn$^{2+/3+}$, Fe$^{2+/3+}$, and Ni$^{2+/3+}$). We did not consider cobalt as a redox center due to its high cost and low abundance.[3] Notably, the electrochemistry of 19 of these 21 compounds has not previously been reported (except for $K_6V_2(PO_4)_4$ which was published while we conducted this study[43]). Next, a capacity filter (>100 mA h g^{-1} based on K and TM oxidation ability) was applied, and 10 compounds with promising theoretical capacity were identified and are listed in Table 1. The approximate voltage profiles of the 10 entries were calculated, and only four of them were found to have an average voltage <4.5 V. Our experimental investigation therefore first focused on these four compounds. Note that we only considered metals with multi-electron redox capability during the screening process. In principle one can also search for polyanion compounds with redox inactive metals such as Al, Zn, *etc.* and then evaluate the possibility of synthesizing their structure with redox active metals as has been done in some previous more elaborate high-throughput searches.[44,45] However, in this work we limit ourselves to compounds which have already been reported in the ICSD database.

Experimental exploration of four potential K-ion cathodes with reasonable voltage

The four potential K-ion cathode materials of interest were successfully synthesized using conventional solid-state methods (Experimental section) and characterized using XRD. As shown in Fig. 2a, the diffraction patterns match well with the simulated ones with no or little evidence of any impurity phases. Fig. 2b summarizes the calculated voltage profiles of the
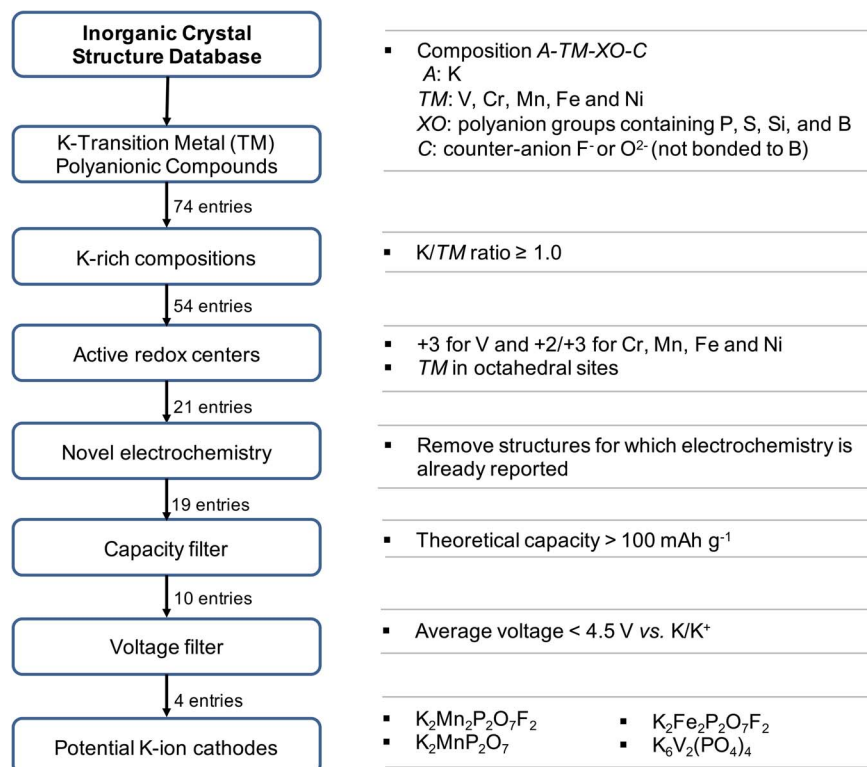
18566 | *J. Mater. Chem. A*, 2021, **9**, 18564–18575

This journal is © The Royal Society of Chemistry 2021

Inorganic Crystal Structure Database

↓

K-Transition Metal (TM) Polyanionic Compounds

- Composition A-TM-XO-C
  A: K
  TM: V, Cr, Mn, Fe and Ni
  XO: polyanion groups containing P, S, Si, and B
  C: counter-anion F^- or O^{2-} (not bonded to B)

↓ 74 entries

K-rich compositions

- K/TM ratio ≥ 1.0

↓ 54 entries

Active redox centers

- +3 for V and +2/+3 for Cr, Mn, Fe and Ni
- TM in octahedral sites

↓ 21 entries

Novel electrochemistry

- Remove structures for which electrochemistry is already reported

↓ 19 entries

Capacity filter

- Theoretical capacity > 100 mAh g^{-1}

↓ 10 entries

Voltage filter

- Average voltage < 4.5 V vs. K/K^+

↓ 4 entries

Potential K-ion cathodes

- $K_2Mn_2P_2O_7F_2$
- $K_2MnP_2O_7$
- $K_2Fe_2P_2O_7F_2$
- $K_6V_2(PO_4)_4$

Fig. 1 Flowchart describing the computational materials search for K-polyanion cathode materials. Following the initial composition screening, the presence of a K-rich composition, an active redox center, a novel electrochemistry, a large theoretical capacity (>100 mA h g^{-1}), and a practical operating voltage (<4.5 V) were used as sequential filters, resulting in 4 potential candidates: $K_2MnP_2O_7$, $K_2Mn_2P_2O_7F_2$, $K_2Fe_2P_2O_7F_2$, and $K_6V_2(PO_4)_4$.

four compounds, i.e., $K_2MnP_2O_7$, $K_2Mn_2P_2O_7F_2$, $K_2Fe_2P_2O_7F_2$, and $K_6V_2(PO_4)_4$, all which exhibit promising theoretical capacity (>100 mA h g^{-1}) at a reasonable operating voltage (<4.5 V). The electrochemical properties of these four compounds as K-ion cathodes were then tested in K metal half-cells with the results plotted in Fig. 2c. For $K_2MnP_2O_7$, $K_2Mn_2P_2O_7F_2$, and $K_2Fe_2P_2O_7F_2$, K ions could be extracted electrochemically; however, the deintercalation process is irreversible with almost no capacity observed during the subsequent discharge. Even when charged to a lower cut-off voltage, no discharge capacity is observed. In contrast, $K_6V_2(PO_4)_4$ delivers about 17% of the charged capacity back in discharge. By decreasing the charge voltage cutoff to 4.0 V, the electrochemical performance of

$K_6V_2(PO_4)_4$ can be improved, as shown in Fig. 2d. Although the first-cycle coulombic efficiency is approximately 50%, a reversible capacity of ~42 mA h g^{-1} with high coulombic efficiency could be obtained during the second cycle. Further lowering the cut-off voltage to 3.75 or 3.25 V significantly reduces the capacity (Fig. S2†).

Experimental investigation of high-voltage $K_3V_{3-x}Cr_x(PO_4)_4$ (x = 0, 1, 2, 3) system

The remaining six compounds in Table 1 identified in the screening show promising theoretical capacity; however, their high predicted operating voltage beyond 4.5 V limits their

Table 1 Ten potential candidates for K-ion cathodes identified from computational screening of the ICSD. The average voltage was determined from the calculated voltage profiles (Fig. S1)

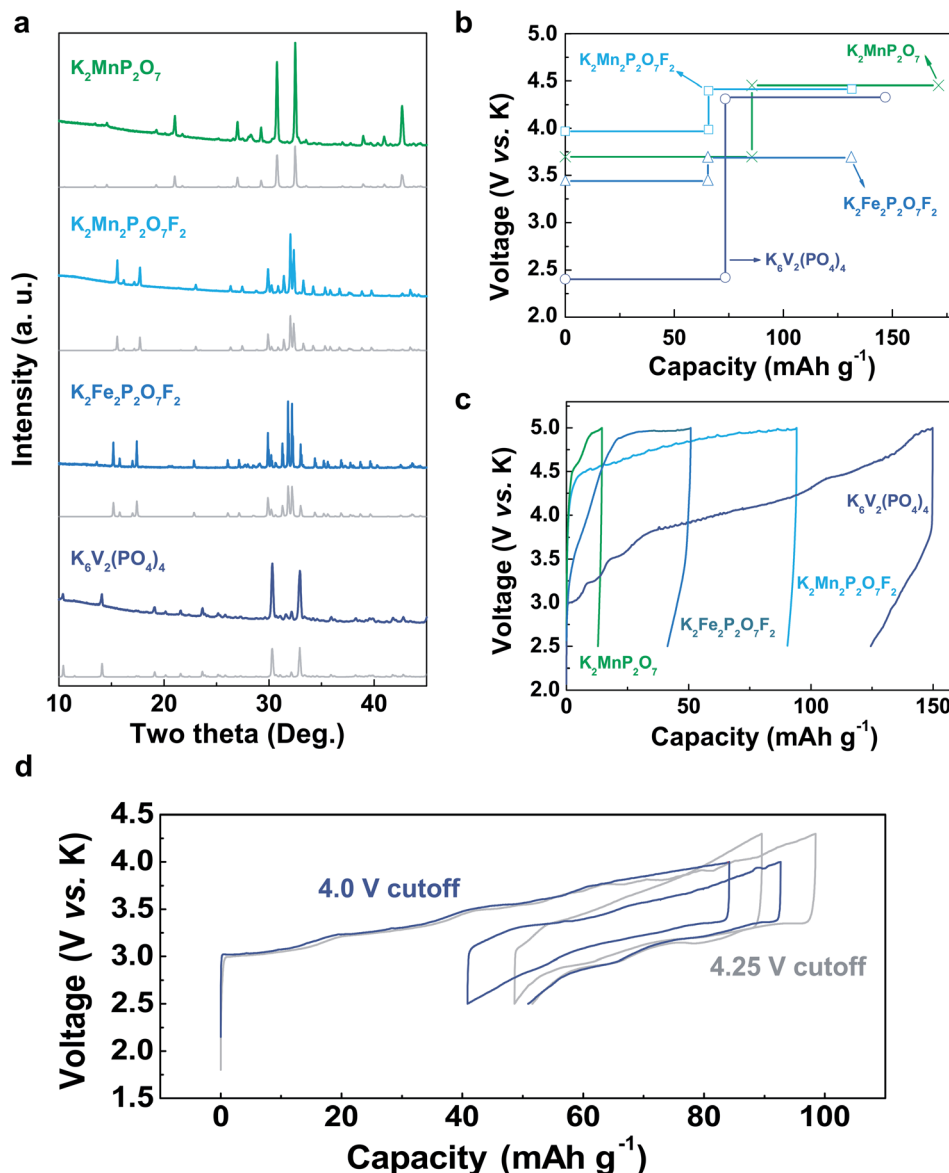| #	Compound	Potential redox couple	Theoretical capacity (mA h g^{-1})	Average voltage (V)
1	$K_2MnP_2O_7$	$Mn^{2+/4+}$	171.2	4.08
2	$K_2Mn_2P_2O_7F_2$	$Mn^{2+/3+}$	131.4	4.19
3	$K_2Fe_2P_2O_7F_2$	$Fe^{2+/3+}$	130.7	3.56
4	$K_6V_2(PO_4)_4$	$V^{3+/5+}$	149.8	3.36
5	$K_3Cr_3(PO_4)_4$	$Cr^{3+/4+}$	120.7	4.85
6	$K_2Mn_2(SO_4)_3$	$Mn^{2+/3+}$	110.4	4.74
7	$K_2Ni_2(SO_4)_3$	$Ni^{2+/3+}$	108.6	5.19
8	$KCrPO_4F$	$Cr^{3+/4+}$	128.2	4.88
9	$KFePO_4F$	$Fe^{3+/4+}$	125.7	5.27
10	$KMnPO_3F_3$	$Mn^{3+/4+}$	114.3	5.55

Fig. 2 XRD patterns and electrochemical properties of four potential K-ion cathodes. (a) Experimentally observed (top line) and simulated XRD patterns (bottom line). (b) Calculated approximate voltage profiles. The plateaus reflect the fact that only an average voltage between each two successive K-contents is calculated. Voltage profiles of all predicted compounds are shown in Fig. S1.† (c) Electrochemical voltage profiles in K-metal half-cells between 2.5 and 5 V at a current density of 5 mA g^{-1}. (d) 1st and 2nd cycle voltage profiles of $K_6V_2(PO_4)_4$ with cut-off voltage of 4.25 and 4.0 V.

practical application. The operating voltage in a polyanion system can be tailored by either polyanion substitution or transition-metal substitution.[46–48] In an effort to use these tools, one of the proposed high-voltage compounds, $K_3Cr_3(PO_4)_4$, was further investigated in an attempt to lower its voltage. According to the calculated voltage profiles in Fig. S1,† the extraction of the last two K ions occurs above 5 V in this compound. We evaluated the effect of V substitution because $V^{3+/4+}$ redox typically occurs at lower voltage than $Cr^{3+/4+}$ redox in polyanion compounds,[46,47,49] and several V-based polyanionic K cathodes have shown reasonable working voltage.[20,23,25–28,30,31] Indeed, we observe a decreased voltage in the calculated voltage profiles of the V-substituted $K_3Cr_3(PO_4)_4$ compounds (Fig. S3†). Therefore,

V^{3+} substitution for Cr^{3+} was performed experimentally and a series of $K_3V_{3-x}Cr_x(PO_4)_4$ ($x = 0, 1, 2, 3$) compounds were successfully synthesized via solid-state method and electrochemically evaluated.

Fig. 3a presents the XRD pattern of $K_3V_3(PO_4)_4$ together with the refinement results. The refined structure of $K_3V_3(PO_4)_4$ belongs to the orthorhombic space group *Cmca*, and is isostructural to $K_3Cr_3(PO_4)_4$.[50] The refined lattice parameters are $a = 10.734$ (5) Å, $b = 20.41$ (1) Å, and $c = 6.502$ (3) Å. The XRD patterns of $K_3V_2Cr(PO_4)_4$, $K_3VCr_2(PO_4)_4$, and $K_3Cr_3(PO_4)_4$ are similar to that of $K_3V_3(PO_4)_4$, as shown in Fig. 3b, except for a slight, non-uniform shift of the diffraction peaks (inset of Fig. 3b). Fig. 3c–f summarize the refined volume and lattice

18568 | *J. Mater. Chem. A*, 2021, **9**, 18564–18575

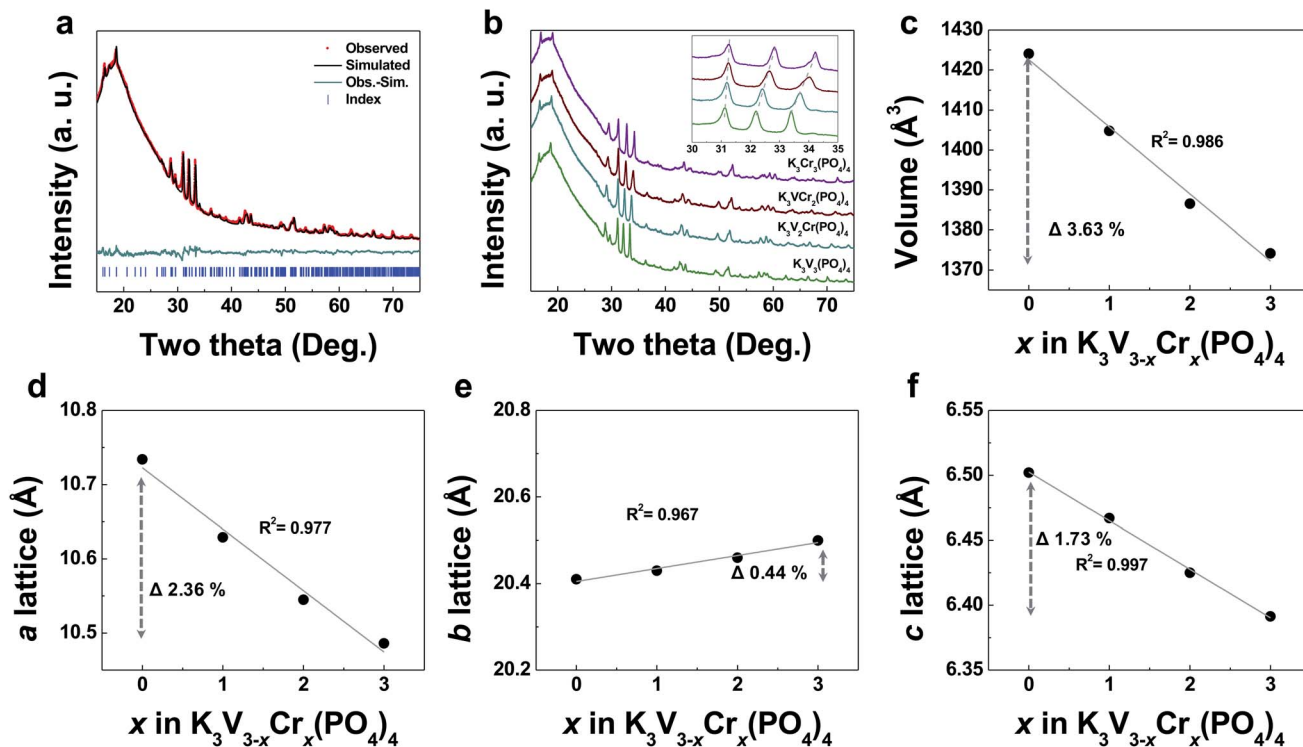This journal is © The Royal Society of Chemistry 2021

Fig. 3 XRD analysis of $K_3V_{3-x}Cr_x(PO_4)_4$ ($x = 0, 1, 2, 3$). (a) Refinement result of $K_3V_3(PO_4)_4$. (b) XRD patterns of $K_3V_3(PO_4)_4$, $K_3V_2Cr(PO_4)_4$, $K_3VCr_2(PO_4)_4$, and **$K_3Cr_3(PO_4)_4$**. (c) Volume and (d) a, (e) b, and (f) c lattice parameters of $K_3V_{3-x}Cr_x(PO_4)_4$ ($x = 0, 1, 2, 3$) obtained from refinements in Fig. S4.† The high-intensity bump in (a and b) at low angle is from the background of Kapton tape.

parameters for $K_3V_{3-x}Cr_x(PO_4)_4$ ($x = 0, 1, 2, 3$). A continuous change with respect to the V : Cr ratio can be clearly observed, indicating the successful incorporation of V^{3+}. As expected, the

a and c lattice parameters monotonically decrease by 2.36% and 1.73%, respectively, with the increasing content of the smaller-sized Cr^{3+}. In contrast, the b lattice parameter remains relatively
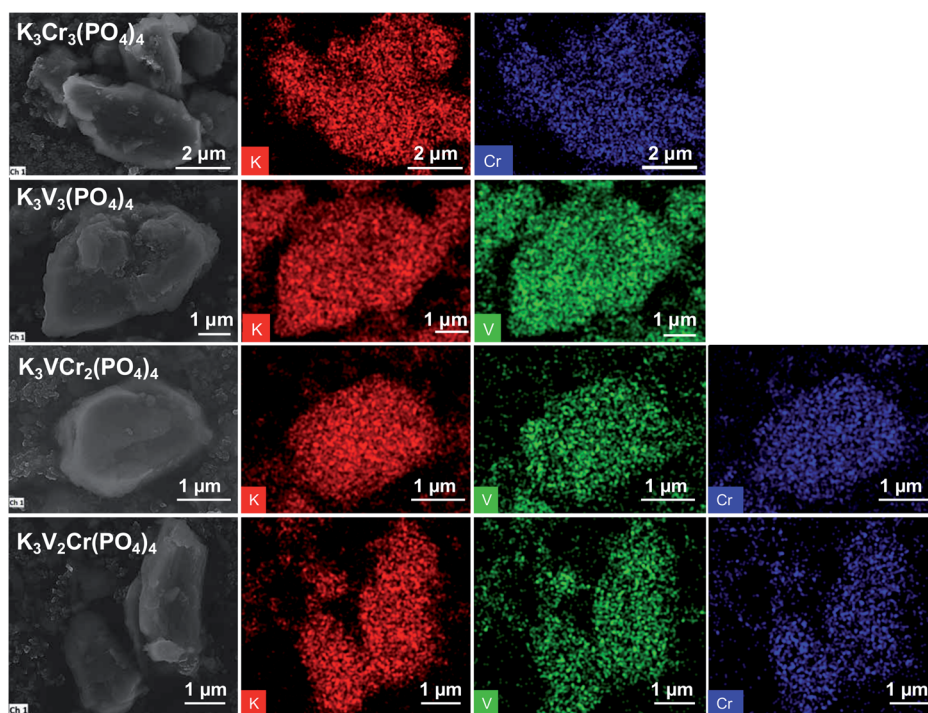
Fig. 4 SEM and EDS mapping images. From top to bottom: **$K_3Cr_3(PO_4)_4$**, $K_3V_3(PO_4)_4$, $K_3VCr_2(PO_4)_4$, and $K_3V_2Cr(PO_4)_4$.
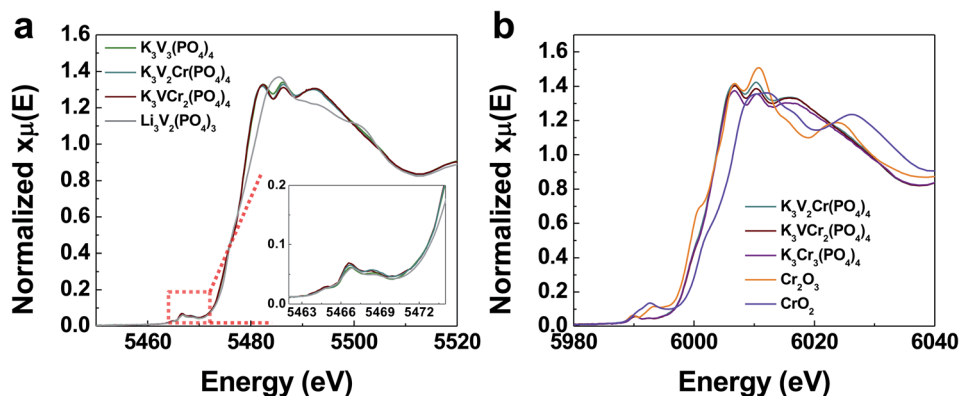
Fig. 5 XANES spectra of $K_3V_3(PO_4)_4$, $K_3V_2Cr(PO_4)_4$, $K_3VCr_2(PO_4)_4$, and **$K_3Cr_3(PO_4)_4$**. (a) V K-edge (b) Cr K-edge. $Li_3V_2(PO_4)$, Cr_2O_3, and CrO_2 are used as references for V^{3+}, Cr^{3+}, and Cr^{4+}, respectively.

constant (0.44% change). As a result, the overall volume decreases by 3.63%. Detailed refinement results are presented in Fig. S4.† In all four compounds, there is no noticeable formation of any impurity phase. In addition, Fig. 4 shows the elemental distributions in as-synthesized particles obtained from energy dispersive X-ray spectroscopy (EDS), further confirming that K, V, and Cr are homogenously distributed within particles without any phase segregation. The particle size of $K_3V_{3-x}Cr_x(PO_4)_4$ ($x = 0, 1, 2, 3$) as determined from scanning electron microscopy (SEM) images (Fig. S5†) are similar around a few microns (1–5 μm).

X-ray absorption near edge structure (XANES) spectroscopy was performed to identify the oxidation states of vanadium and

chromium in the as-synthesized $K_3V_{3-x}Cr_x(PO_4)_4$ ($x = 0, 1, 2, 3$) system. Fig. 5a presents the V K-edge spectra of $K_3V_3(PO_4)_4$, $K_3V_2Cr(PO_4)_4$, and $K_3VCr_2(PO_4)_4$. In addition to the identical edge positions and pre-edge features in all three samples, the obtained spectra also overlap with that of the $Li_3V_2(PO_4)_3$ (V^{3+}) reference,[51] confirming that all the $K_3V_{3-x}Cr_x(PO_4)_4$ ($x = 0, 1, 2$) compounds contains V^{3+} in the pristine structure. For the Cr K-edge, no noticeable differences were observed among $K_3V_2Cr(PO_4)_4$, $K_3VCr_2(PO_4)_4$, and **$K_3Cr_3(PO_4)_4$**, and the edge position of all the samples is similar to that of Cr_2O_3, as shown in Fig. 5b. Notably, Cr^{4+} with d^2 electron configuration usually has a distorted octahedral symmetry, which results in a prominent pre-edge peak, as shown by the XAS spectra of CrO_2
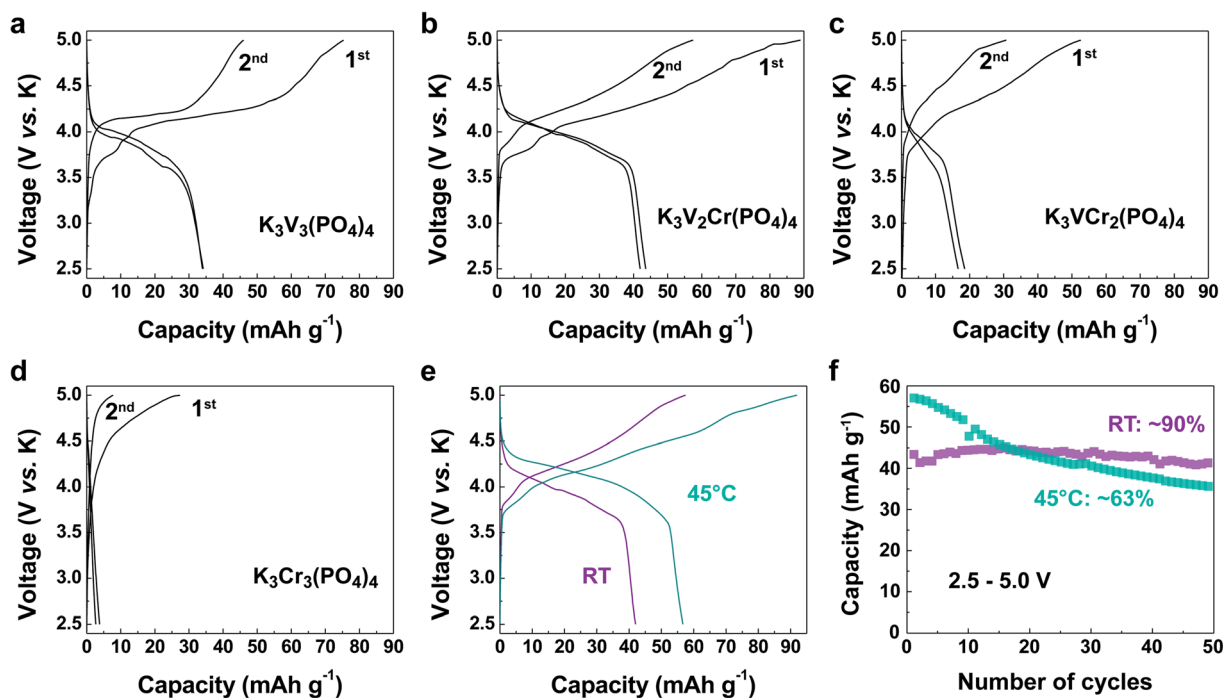

Fig. 6 Electrochemical properties of $K_3V_{3-x}Cr_x(PO_4)_4$ ($x = 0, 1, 2, 3$). First and second charge–discharge profiles between 2.5 and 5.0 V at 10 mA g^{-1} for (a) $K_3V_3(PO_4)_4$, (b) $K_3V_2Cr(PO_4)_4$, (c) $K_3VCr_2(PO_4)_4$, and (d) **$K_3Cr_3(PO_4)_4$**. (e) Voltage profiles of $K_3V_2Cr(PO_4)_4$ at room temperature and 45 °C. (f) Cycling stability of $K_3V_2Cr(PO_4)_4$ at room temperature and 45 °C.

18570 | *J. Mater. Chem. A*, 2021, **9**, 18564–18575
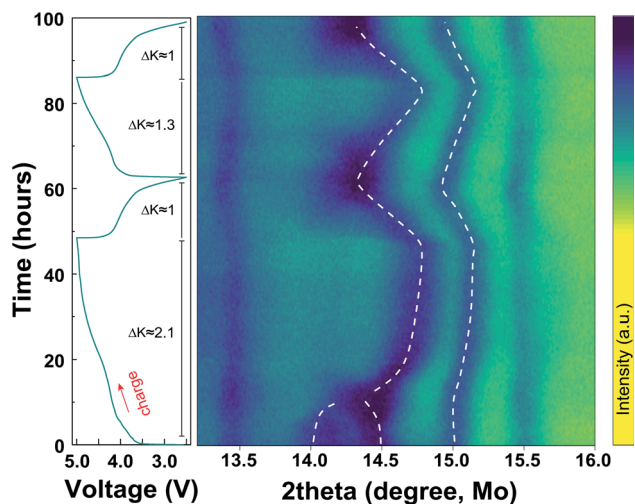
This journal is © The Royal Society of Chemistry 2021

Fig. 7 Structural evolution of $K_3V_2Cr(PO_4)_4$ monitored by *in situ* XRD. The electrochemical charge–discharge profile of the $K_3V_2Cr(PO_4)_4$ cathode cycled at 3 mA g^{-1} between 2.5 and 5.0 V is shown on the left, and the corresponding *in situ* XRD pattern is plotted in a contour style on the right. Dark color indicates higher intensity. The evolution of the main peaks is highlighted with white dashed lines.

reference.[46,47] However, no such pre-edge feature is observed for any of the $K_3V_{3-x}Cr_x(PO_4)_4$ ($x = 1, 2, 3$) compounds, indicating that Cr is present as Cr^{3+} in all the samples.

The $K_3V_{3-x}Cr_x(PO_4)_4$ ($x = 0, 1, 2, 3$) samples were tested in K-half cells, with K metal and 0.7 M KPF_6 in EC/PC (1 : 1 vol.) used as the anode and electrolyte, respectively. The first and second charge–discharge profiles of all four compounds are presented in Fig. 6a–d. During the first charge all the samples exhibit some irreversible capacity which may originate from the electrolyte decomposition because of the high cut-off voltage (5.0 V *vs.* K/K$^+$). For discharge, $K_3V_2Cr(PO_4)_4$ delivers the highest discharge capacity of $\sim$43 mA h g^{-1} with an average voltage of 3.95 V, followed by $K_3V_3(PO_4)_4$ ($\sim$34 mA h g^{-1} and 3.85 V), $K_3VCr_2(PO_4)_4$ ($\sim$17 mA h g^{-1} and 3.77 V), and **$K_3Cr_3(PO_4)_4$** ($\sim$3 mA h g^{-1} and 3.46 V).

When the temperature increases to 45 °C, as shown in Fig. 6e, the $K_3V_2Cr(PO_4)_4$ cathode exhibits smaller polarization

and delivers a higher discharge capacity of $\sim$57 mA h g^{-1}, indicating that poor K-ion diffusion may limit the room temperature performance. Although the electrochemical cycling at 45 °C increases the specific capacity, the cycling stability becomes worse: only 63% of the discharge capacity remains after 50 cycles compared with 90% at room temperature (Fig. 6f), which can likely be attributed to the accelerated electrolyte decomposition at higher temperature.[52]

As it shows the highest capacity among the $K_3V_{3-x}Cr_x(PO_4)_4$ systems, the structure of $K_3V_2Cr(PO_4)_4$ was monitored by *in situ* XRD upon K (de)intercalation. Fig. 7 presents the *in situ* XRD patterns obtained from $K_3V_2Cr(PO_4)_4$ cycled between 2.5 and 5.0 V in a K-half cell. Upon the first charge, the peaks at 14.0° and 14.5° merge into one peak at 14.3°. Further charge shifts the peaks at 14.3° and 15° to higher angle, consistent with a shrinkage of the lattice upon K extraction. Apart from the continuous peak shift, no additional peak evolution is observed, indicating that K-extraction from $K_3V_2Cr(PO_4)_4$ occurs *via* a solid solution. Upon discharge, the peaks at 14.7° and 15.2° shift to lower angle, corresponding to an expansion of the lattice by K insertion. However, at the end of the discharge, the peak at 14.3° does not split into two peaks as in the XRD pattern of the pristine structure. This irreversible structural behavior could be the result of low K diffusivity in the discharged state, which is often observed in the literature.[16] During the second cycle, a continuous peak shift is again observed, demonstrating that, after the first cycle, K extraction and reinsertion occur reversibly in $K_3V_2Cr(PO_4)_4$.

To understand the redox mechanism in $K_3V_2Cr(PO_4)_4$ during K (de)intercalation, we monitored the valence change of V and Cr during charge–discharge *via ex situ* XANES spectroscopy. Fig. 8a shows the V K-edge, and the inset shows the enlarged pre-edge feature. The intensity of the pre-edge peak at $\sim$5469 eV significantly increases when the cathode is charged to 4.5 V and further increases at 5.0 V, clearly indicating the oxidation of V^{3+} to V^{4+}.[53] After discharging, the pre-edge peak intensity at $\sim$5469 eV decreases to close to that of the pristine $K_3V_2Cr(PO_4)_4$, indicating a reversible but incomplete reduction of V^{4+} to V^{3+}. In the second cycle, reversible V oxidation and reduction are also observed. In contrast, no change is observed in the Cr K-edge, as
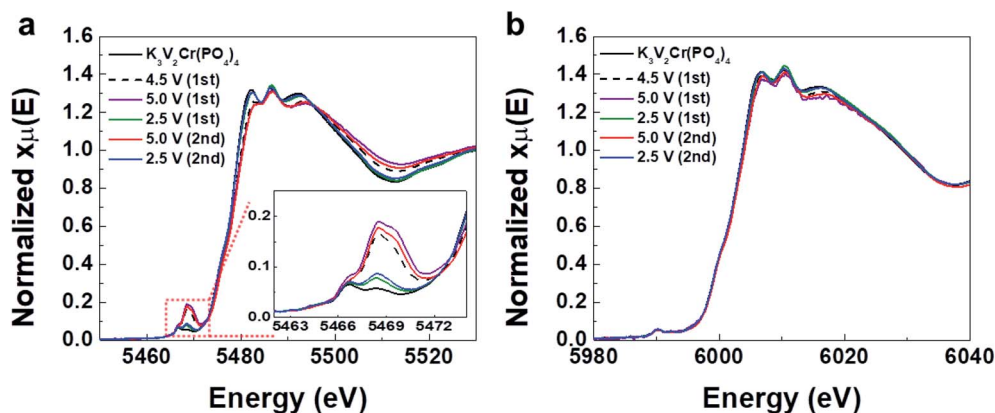

Fig. 8 XANES spectra of $K_3V_2Cr(PO_4)_4$ at various charge states. (a) V K-edge and (b) Cr K-edge.

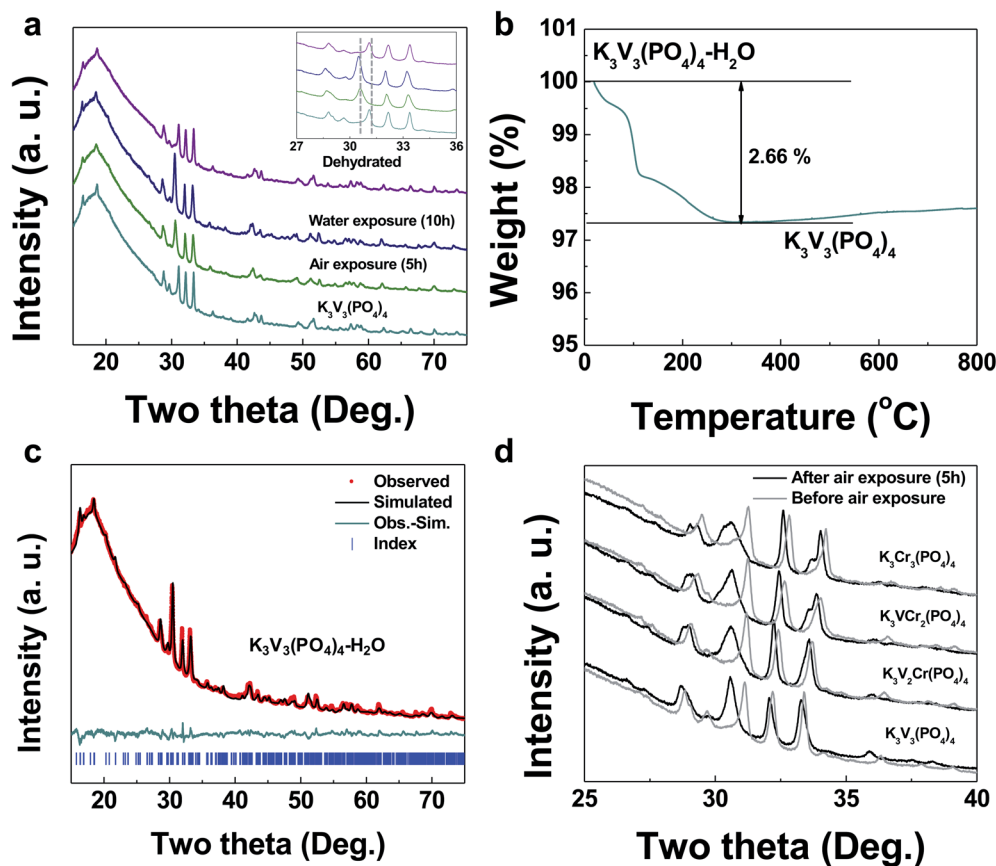**Fig. 9** Hydration and dehydration analysis of $K_3V_{3-x}Cr_x(PO_4)_4$ ($x = 0, 1, 2, 3$) compounds. (a) XRD patterns of $K_3V_3(PO_4)_4$ after air exposure, water exposure, and dehydration. (b) Thermal analysis result for hydrated $K_3V_3(PO_4)_4$. (c) XRD refinement result for $K_3V_3(PO_4)_4–H_2O$. (d) XRD patterns of $K_3V_3(PO_4)_4$, $K_3V_2Cr(PO_4)_4$, $K_3VCr_2(PO_4)_4$, and $K_3Cr_3(PO_4)_4$ before and after air exposure.

shown in Fig. 8b. This finding implies that Cr does not participate in the redox reaction in this compound.

We found that $K_3V_{3-x}Cr_x(PO_4)_4$ ($x = 0, 1, 2, 3$) compounds are easily hydrated, as demonstrated by the difference in the XRD patterns after hydration and dehydration in Fig. 9a. When exposed to air or water, the XRD peak at ∼31° disappears and a new peak emerges at ∼30.5°. After dehydration at 600 °C, the pristine diffraction pattern could be recovered. Fig. 9b presents the weight change of the hydrated compound upon heating; ∼2.66% weight loss is observed, corresponding to $1H_2O$ per formula unit of $K_3V_3(PO_4)_4$. Moreover, the crystal structure of the hydrated compound $K_3V_3(PO_4)_4–H_2O$ was furthered analyzed, and the refinement result is presented in Fig. 9c. An orthorhombic $K_3Fe_3(PO_4)_4–H_2O$ (space group: *Pnna*)[54,55] was used as a model structure and shows good agreement with the observed XRD pattern. The XRD pattern of the hydrated phase also fits well with a very recent report of orthorhombic $K_3V_3(PO_4)_4–H_2O$.[56] Similarly, all the $K_3V_{3-x}Cr_x(PO_4)_4$ ($x = 0, 1, 2, 3$) compounds exhibit such hydration behavior, as evidenced by the peak change at approximately 30° after 5 h air exposure (Fig. 9d). The moisture sensitive nature of $K_3V_{3-x}Cr_x(PO_4)_4$ ($x = 0, 1, 2, 3$) requires an inert storage environment of these materials, which might lead to difficulty in applications.

Discussion

The average voltage of several K layered and polyanion cathodes as well as their experimentally reported Li or Na analogous are plotted in Fig. 10. Due to the steepness of the voltage profiles, K layered oxides suffer a significant voltage lowering when
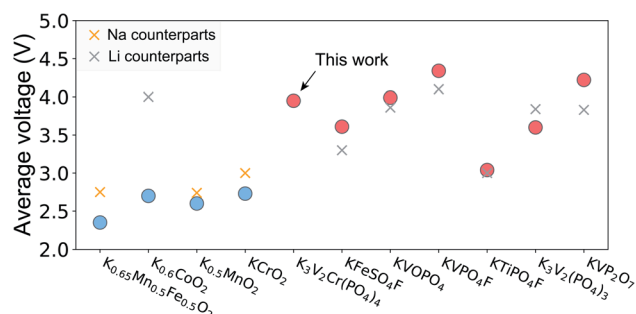

Fig. 10 Average discharge voltage of various K-ion cathodes. K layered oxides are represented by blue circles, and K polyanions are represented by red circles. The corresponding Li (grey cross) and Na (yellow cross) counterparts, *i.e.*, $Na_{0.66}Fe_{0.5}Mn_{0.5}O_2$, $LiCoO_2$, $NaMnO_2$, $NaCrO_2$, $LiFeSO_4F$, $LiVOPO_4$, $LiVPO_4F$, $LiTiPO_4F$, $Li_3V_2(PO_4)_3$, and $LiVP_2O_7$, are also included for comparison.[8,13,18,57–62]

18572 | *J. Mater. Chem. A*, 2021, **9**, 18564–18575

This journal is © The Royal Society of Chemistry 2021

Table 2 DFT-calculated volume change and energy above the hull of the four predicted compounds upon K extraction

Compound	Volume change (%)		E_{hull} (meV per atom)		
	Half extraction	Full extraction	Pristine	Half extraction	Full extraction
$K_2MnP_2O_7$	−11.3	−21.5	0.14	15.91	36.10
$K_2Mn_2P_2O_7F_2$	−5.9	−12.4	1.33	10.22	21.70
$K_2Fe_2P_2O_7F_2$	−4.2	−9.6	0	12.02	14.47
$K_6V_2(PO_4)_4$	−3.7	−6.0	0	17.27	62.69

compared with their Li counterparts: for example, $LiCoO_2$ exhibits an average voltage of approximately 4 V, which is ~1.3 V higher than that of $K_{0.6}CoO_2$.[11] Moreover, the voltage of K layered oxides is also lower than that of Na layered oxides, which makes K layered oxides even less competitive in terms of energy density.[18] In contrast, our work confirms the general finding that polyanion systems have less sloped voltage profile compared to that of layered oxide, which makes higher operating voltage in K polyanion systems possible. Despite their more optimal voltage profile, the $K_3V_{3-x}Cr_x(PO_4)_4$ systems are not satisfactory from an energy density perspective because of the low specific capacity.

K-containing polyanion systems seem to have a remarkably high voltage for a given redox couple. As shown in Table 1, only 4 of the 10 predicted materials have a reasonable average voltage. Although most of the reported K polyanion cathodes are based on $V^{3+/4+}$, $Fe^{2+/3+}$, or $Ti^{3+/4+}$ redox couples, which one would expect to have relatively low redox potential, their operating voltage approaches or even surpasses 4 V.[20,27,32,34] In particular, as shown in Fig. 10, the voltages of $KFeSO_4F$, $KVOPO_4$, $KVPO_4F$, $KTiPO_4F$, and KVP_2O_7 are even higher than those of their Li counterparts. This is likely due to the large site energy of K^+, since the large K^+ ion tends to have a larger coordination number, as observed in our materials. As a result, the high voltage at which redox couples function in a K polyanion structure to some extent limits the use of many redox couples; for example, $Mn^{2+/4+}$, $Ni^{2+/4+}$, and $V^{3+/5+}$ double redox is unlikely to be fully utilized in a practical voltage window. It might be worthwhile to understand better how structure and composition can be tuned to lower the voltage in a compound.

We find that some of the proposed compounds suffer from a significant amount of first-cycle irreversible capacity. To investigate the origin of the irreversibility of the proposed compounds, the volume change and calculated energy above the hull of $K_2MnP_2O_7$, $K_2Mn_2P_2O_7F_2$, $K_2Fe_2P_2O_7F_2$, and $K_6V_2(PO_4)_4$ upon K extraction are summarized and presented in Table 2. Apart from $K_2MnP_2O_7$, which undergoes a large volume change of 21.5%, the volume reduction of the other compounds in the full de-intercalation range is comparable or only slightly larger than that of several reported working K polyanion cathodes (e.g., $KTiPO_4F$: 9.0%, $KVPO_4F$: 6.54%, $K_3V_2(PO_4)_3$: 3.8%).[20,34,63] Moreover, the energy above the hull for the charged states show a certain amount of driving force to decompose to other phases, but is not fundamentally different from that for charged Li or Na cathode materials. Therefore, it is unlikely that

the electrochemical irreversibility is induced by a structural instability in the charged state.

The fact that substantially higher capacity is achieved when $K_3V_2Cr(PO_4)_4$ is cycled at 45 °C indicates a diffusion limitation, which seems plausible for K^+ because of its extremely large size. As an example, we performed a climbing image Nudged Elastic Band (NEB) calculation for K^+ migration in $K_2MnP_2O_7$ and found that the energy barrier varies from 1.49 eV to 2.91 eV depending on the K concentration per formula unit (Fig. S6†), which is consistent with the negligible capacity as observed in Fig. 2. Moreover, a polyanion compound typically has poor electronic conductivity, which may limit the achievable specific capacity. In such cases, proper carbon coating or preparing active material–carbon matrix composite might be helpful to improve the electrochemical performance. For example, in a very recent paper by Bodart et al., it was demonstrated that the capacity of $K_6V_2(PO_4)_4$ can be doubled or even tripled by the in situ addition of conductive carbon during the synthesis process and thorough grinding.[43] In addition, the high cutoff voltage needed to access the high oxidation energies for the TM redox couples likely contributes to electrolyte degradation and the potential formation of an insulating solid-electrolyte interphases.[20,29] Therefore, although $K_2MnP_2O_7$, $K_2Mn_2P_2O_7F_2$, $K_2Fe_2P_2O_7F_2$, and $K_6V_2(PO_4)_4$ do not show high specific capacity under the conditions currently explored, further improvement in energy density may remain feasible through optimization of the synthesis method, particle morphology and electrolyte.

Conclusion

In conclusion, ten potential K polyanion cathodes with >100 mA h g^{-1} theoretical capacity are identified from the computational screening of the ICSD, among which four compounds ($K_2MnP_2O_7$, $K_2Mn_2P_2O_7F_2$, $K_2Fe_2P_2O_7F_2$, $K_6V_2(PO_4)_4$) and a family of $K_3V_{3-x}Cr_x(PO_4)_4$ ($x = 0, 1, 2, 3$) compounds are synthesized and explored electrochemically. Among these, $K_3V_2Cr(PO_4)_4$ delivers the largest reversible capacity, and the redox mechanism and structural evolution are further investigated via X-ray absorption and diffraction techniques, respectively. Though K polyanion compounds presented in this work indeed show less sloped voltage profiles compared to layered oxides, other issues such as high K ions migration barrier, high oxidation voltage bring up new challenges, which calls for more in-depth electrochemical investigation and composition engineering in the future.

This journal is © The Royal Society of Chemistry 2021

J. Mater. Chem. A, 2021, **9**, 18564–18575 | **18573**

Author contributions

Conflicts of interest

Acknowledgements

References

1 N. Yabuuchi and S. Komaba, *Sci. Technol. Adv. Mater.*, 2014, **15**, 043501.

2 Y. Li, Y. Lu, C. Zhao, Y.-S. Hu, M.-M. Titirici, H. Li, X. Huang and L. Chen, *Energy Storage Mater.*, 2017, **7**, 130–151.

3 X. Fu, D. N. Beatty, G. G. Gaustad, G. Ceder, R. Roth, R. E. Kirchain, M. Bustamante, C. Babbitt and E. A. Olivetti, *Environ. Sci. Technol.*, 2020, **54**, 2985–2993.

4 H. Kim, J. C. Kim, M. Bianchini, D. H. Seo, J. Rodriguez-Garcia and G. Ceder, *Adv. Energy Mater.*, 2018, **8**, 1702384.

5 J. Zhao, X. Zou, Y. Zhu, Y. Xu and C. Wang, *Adv. Funct. Mater.*, 2016, **26**, 8103–8110.

6 S. Komaba, T. Hasegawa, M. Dahbi and K. Kubota, *Electrochem. Commun.*, 2015, **60**, 172–175.

7 M. Okoshi, Y. Yamada, S. Komaba, A. Yamada and H. Nakai, *J. Electrochem. Soc.*, 2016, **164**, A54.

8 H. Kim, H. Ji, J. Wang and G. Ceder, *Trends Chem.*, 2019, **1**, 682–692.

9 N. Naveen, S. C. Han, S. P. Singh, D. Ahn, K.-S. Sohn and M. Pyo, *J. Power Sources*, 2019, **430**, 137–144.

10 H. Kim, D. H. Seo, J. C. Kim, S. H. Bo, L. Liu, T. Shi and G. Ceder, *Adv. Mater.*, 2017, **29**, 1702480.

11 H. Kim, J. C. Kim, S. H. Bo, T. Shi, D. H. Kwon and G. Ceder, *Adv. Energy Mater.*, 2017, **7**, 1700098.

12 X. Zhang, Y. Yang, X. Qu, Z. Wei, G. Sun, K. Zheng, H. Yu and F. Du, *Adv. Funct. Mater.*, 2019, **29**, 1905679.

13 T. Deng, X. Fan, J. Chen, L. Chen, C. Luo, X. Zhou, J. Yang, S. Zheng and C. Wang, *Adv. Funct. Mater.*, 2018, **28**, 1800219.

14 C. Vaalma, G. A. Giffin, D. Buchholz and S. Passerini, *J. Electrochem. Soc.*, 2016, **163**, A1295.

15 Y. Hironaka, K. Kubota and S. Komaba, *Chem. Commun.*, 2017, **53**, 3693–3696.

16 H. Kim, D.-H. Seo, A. Urban, J. Lee, D.-H. Kwon, S.-H. Bo, T. Shi, J. K. Papp, B. D. McCloskey and G. Ceder, *Chem. Mater.*, 2018, **30**, 6532–6539.

17 T. Masese, K. Yoshii, Y. Yamaguchi, T. Okumura, Z.-D. Huang, M. Kato, K. Kubota, J. Furutani, Y. Orikasa and H. Senoh, *Nat. Commun.*, 2018, **9**, 1–12.

18 Y. Tian, G. Zeng, A. Rutt, T. Shi, H. Kim, J. Wang, J. Koettgen, Y. Sun, B. Ouyang, T. Chen, Z. Lun, Z. Rong, K. Persson and G. Ceder, *Chem. Rev.*, 2021, **121**(3), 1623–1669.

19 W. Lee, J. Kim, S. Yun, W. Choi, H. Kim and W.-S. Yoon, *Energy Environ. Sci.*, 2020, **13**(12), 4406–4449.

20 H. Kim, D. H. Seo, M. Bianchini, R. J. Clément, H. Kim, J. C. Kim, Y. Tian, T. Shi, W. S. Yoon and G. Ceder, *Adv. Energy Mater.*, 2018, **8**, 1801591.

21 M. D. Radin and A. Van der Ven, *Chem. Mater.*, 2016, **28**, 7898–7904.

22 S. S. Fedotov, N. R. Khasanova, A. S. Samarin, O. A. Drozhzhin, D. Batuk, O. M. Karakulina, J. Hadermann, A. M. Abakumov and E. V. Antipov, *Chem. Mater.*, 2016, **28**, 411–415.

23 J. Han, G.-N. Li, F. Liu, M. Wang, Y. Zhang, L. Hu, C. Dai and M. Xu, *Chem. Commun.*, 2017, **53**, 1805–1808.

24 H. He, W. Yao, S. Tunmee, X. Zhou, B. Ji, N. Wu, T. Song, P. Kidkhunthod and Y. Tang, *J. Mater. Chem. A*, 2020, **8**, 9128–9136.

25 X. Lin, J. Huang, H. Tan, J. Huang and B. Zhang, *Energy Storage Mater.*, 2019, **16**, 97–101.

26 W. B. Park, S. C. Han, C. Park, S. U. Hong, U. Han, S. P. Singh, Y. H. Jung, D. Ahn, K. S. Sohn and M. Pyo, *Adv. Energy Mater.*, 2018, **8**, 1703099.

27 K. Chihara, A. Katogi, K. Kubota and S. Komaba, *Chem. Commun.*, 2017, **53**, 5208–5211.

28 J. Liao, Q. Hu, X. He, J. Mu, J. Wang and C. Chen, *J. Power Sources*, 2020, **451**, 227739.

29 H. Kim, Y. Tian and G. Ceder, *J. Electrochem. Soc.*, 2020, **167**, 110555.

30 Z. Liu, J. Wang and B. Lu, *Sci. Bull.*, 2020, **65**(15), 1242–1251.

31 T. Hosaka, T. Shimamura, K. Kubota and S. Komaba, *Chem. Rec.*, 2019, **19**, 735–745.

32 N. Recham, G. l. Rousse, M. T. Sougrati, J.-N. l. Chotard, C. Frayret, S. Mariyappan, B. C. Melot, J.-C. Jumas and J.-M. Tarascon, *Chem. Mater.*, 2012, **24**, 4363–4370.

33 S. S. Fedotov, A. S. Samarin, V. A. Nikitina, D. A. Aksyonov, S. A. Sokolov, A. Zhugayevych, K. J. Stevenson,

18574 | *J. Mater. Chem. A*, 2021, **9**, 18564–18575

This journal is © The Royal Society of Chemistry 2021

N. R. Khasanova, A. M. Abakumov and E. V. Antipov, *J. Mater. Chem. A*, 2018, **6**, 14420–14430.

34 S. S. Fedotov, N. D. Luchinin, D. A. Aksyonov, A. V. Morozov, S. V. Ryazantsev, M. Gaboardi, J. R. Plaisier, K. J. Stevenson, A. M. Abakumov and E. V. Antipov, *Nat. Commun.*, 2020, **11**, 1–11.

35 A. K. Padhi, K. S. Nanjundaswamy and J. B. Goodenough, *J. Electrochem. Soc.*, 1997, **144**, 1188.

36 G. Kresse and J. Furthmüller, *Comput. Mater. Sci.*, 1996, **6**, 15–50.

37 G. Kresse and D. Joubert, *Phys. Rev. B: Condens. Matter Mater. Phys.*, 1999, **59**, 1758.

38 S. Dudarev, G. Botton, S. Savrasov, C. Humphreys and A. Sutton, *Phys. Rev. B: Condens. Matter Mater. Phys.*, 1998, **57**, 1505.

39 L. Wang, T. Maxisch and G. Ceder, *Phys. Rev. B: Condens. Matter Mater. Phys.*, 2006, **73**, 195107.

40 M. Aydinol and G. Ceder, *J. Electrochem. Soc.*, 1997, **144**, 3832.

41 G. Henkelman, B. P. Uberuaga and H. Jónsson, *J. Chem. Phys.*, 2000, **113**, 9901–9904.

42 A. Belsky, M. Hellenbrandt, V. L. Karen and P. Luksch, *Acta Crystallogr., Sect. B: Struct. Sci.*, 2002, **58**, 364–369.

43 J. Bodart, N. Eshraghi, T. Carabin, B. Vertruyen, R. Cloots, F. Boschini and A. Mahmoud, *J. Power Sources*, 2020, **480**, 229057.

44 Y. Wu, P. Lazic, G. Hautier, K. Persson and G. Ceder, *Energy Environ. Sci.*, 2013, **6**, 157–168.

45 G. Hautier, A. Jain, H. Chen, C. Moore, S. P. Ong and G. Ceder, *J. Mater. Chem.*, 2011, **21**, 17147–17153.

46 K. Kawai, W. Zhao, S.-i. Nishimura and A. Yamada, *ACS Appl. Energy Mater.*, 2018, **1**, 928–931.

47 J. Wang, Y. Wang, D. H. Seo, T. Shi, S. Chen, Y. Tian, H. Kim and G. Ceder, *Adv. Energy Mater.*, 2020, **10**, 1903968.

48 A. Padhi, K. Nanjundaswamy, C. Masquelier, S. Okada and J. Goodenough, *J. Electrochem. Soc.*, 1997, **144**, 1609.

49 Z. Jian, W. Han, X. Lu, H. Yang, Y.-S. Hu, J. Zhou, Z. Zhou, J. Li, W. Chen, D. Chen and L. Chen, *Adv. Energy Mater.*, 2013, **3**, 156–160.

50 S. Kouass and H. Boughzala, *Phosphorus, Sulfur Silicon Relat. Elem.*, 2006, **181**, 2641–2652.

51 J. Yoon, S. Muhammad, D. Jang, N. Sivakumar, J. Kim, W.-H. Jang, Y.-S. Lee, Y.-U. Park, K. Kang and W.-S. Yoon, *J. Alloys Compd.*, 2013, **569**, 76–81.

52 C. L. Campion, W. Li and B. L. Lucht, *J. Electrochem. Soc.*, 2005, **152**, A2327.

53 Z. Yang, G. Li, J. Sun, L. Xie, Y. Jiang, Y. Huang and S. Chen, *Energy Storage Mater.*, 2020, **25**, 724–730.

54 K.-H. Lii, *Eur. J. Solid State Inorg. Chem.*, 1995, **32**, 917–926.

55 K. Trad, A. Wattiaux, M. B. Amara, C. Delmas and D. Carlier, *J. Solid State Chem.*, 2018, **262**, 112–120.

56 T. Jenkins, J. A. Alarco and I. D. Mackinnon, *ACS Omega*, 2021, **6**(3), 1917–1929.

57 N. S. Grundish, I. D. Seymour, G. Henkelman and J. B. Goodenough, *Chem. Mater.*, 2019, **31**, 9379–9388.

58 J. Barker, R. Gover, P. Burns, A. Bryan, M. Saidi and J. Swoyer, *J. Power Sources*, 2005, **146**, 516–520.

59 M. Ren, Z. Zhou, L. Su and X. Gao, *J. Power Sources*, 2009, **189**, 786–789.

60 M. Bianchini, N. Brisset, F. Fauth, F. Weill, E. Elkaim, E. Suard, C. Masquelier and L. Croguennec, *Chem. Mater.*, 2014, **26**, 4238–4247.

61 H. Huang, S. C. Yin, T. Kerr, N. Taylor and L. F. Nazar, *Adv. Mater.*, 2002, **14**, 1525–1528.

62 J.-c. Zheng, Y.-d. Han, L.-b. Tang and B. Zhang, *Electrochim. Acta*, 2016, **198**, 195–202.

63 L. Zhang, B. Zhang, C. Wang, Y. Dou, Q. Zhang, Y. Liu, H. Gao, M. Al-Mamun, W. K. Pang and Z. Guo, *Nano Energy*, 2019, **60**, 432–439.

This journal is © The Royal Society of Chemistry 2021

J. Mater. Chem. A, 2021, **9**, 18564–18575 | **18575**